Civil Engineering and Applied Solutions

Research Article

journal homepage: ceas.journals.umz.ac.ir

CEAS Civil Engineering and Applied Solutions

Seismic Behavior and Practical Local Buckling Assessment of Composite Steel Plate Shear Walls

Mehdi Ebadi-Jamkhaneh [a*]

[a] *Department of Civil Engineering, School of Engineering, Damghan University, Damghan, Iran, P.O.BOX: 36716-45667*

ARTICLE INFO

Keywords:
Composite steel plate shear wall
Nonlinear analysis
Earthquake
Shear stud
Concrete panel

Article history:
Received 29 November 2025
Accepted 26 December 2025
Available online 01 July 2026

ABSTRACT

This study investigates the seismic performance of 4- and 6-story composite steel plate shear walls (CSPSWs) using advanced finite element models developed in ABAQUS. The numerical model, rigorously validated against experimental data, was subjected to nonlinear time history analysis under a suite of seven scaled ground motions. The results demonstrate that the design shear strength prescribed by AISC 341-10 is conservative, underestimating the peak dynamic base shear by 28% to 37% for the studied frames. This significant discrepancy is primarily attributed to the substantial shear force resisted by the boundary frame elements and the reinforced concrete panel, contributions not accounted for in the code's simplified methodology. Boundary columns were found to carry up to 26% of the total base shear. Furthermore, the study presents a practical assessment of local buckling in the steel web, proposing a methodological approach for determining shear stud spacing. The analysis confirms that a stud spacing of 300 mm provides a safety margin of 1.7 against buckling before yielding, ensuring the desired energy dissipation mechanism. The research underscores the enhanced seismic resilience of CSPSWs and provides quantitative insights to inform more efficient design practices.

1. Introduction

Composite Steel Plate Shear Walls (CSPSWs) have proven to be an extremely effective lateral force-resisting system, particularly for high-rise buildings in seismic-prone areas. These systems ingeniously combine the advantages of both steel and concrete, overcoming the limitations of using each material individually. A typical CSPSW consists of a steel plate wall that is connected to reinforced concrete panels or infilled with concrete to produce a synergistic system in which the steel plate provides high tensile strength and ductility, while the concrete component prevents or delays the global buckling of the steel plate, thereby enhancing the wall's stiffness and compressive strength [1, 2].

Through seminal experimental work conducted by Zhao and Astaneh-Asl [3], early achievements in validating the cyclic capabilities of composite shear walls were provided through their test work on 3-story half-scale specimens composed of a reinforced concrete wall bolted to a steel plate shear wall. The test series demonstrated high deformation capacity and stable cyclic post-yielding behaviour with the 33 cycles of cyclic shear and drift displacement that the specimens underwent. This maximum drift had a percentage increase of 5%, which was also a crucial finding in the study. The study also highlighted that the function of connectors was to brace the steel plates by providing a composite action, which prevented the steel from buckling as a whole and thus developed a composite effect of the shear wall and reinforced concrete wall combination to develop the highest shear capacity that these systems could develop. The development of inelasticity (localised buckling of the steel plate between the connector bolts) developed during the last cycles of testing and serves to support the principle that composite action is essential to allowing full development of the ductility and high shear capacity that these systems exhibit.

* Corresponding author.
E-mail addresses: m.ebadi@du.ac.ir (M. Ebadi-Jamkhaneh).

https://doi.org/10.22080/ceas.2025.30655.1056
ISSN: 3092-7749/
How to cite this article: Ebadi-Jamkhaneh, M. Seismic Behavior and Practical Local Buckling Assessment of Composite Steel Plate Shear Walls. Civil Engineering and Applied Solutions. 2026; 2(3): 85–95. doi:10.22080/ceas.2025.30655.1056.

In-depth research has advanced several configurations of CSPWS and studied the factors that influence them. Mo et al. [4] conducted a general review of these factors and provided several conclusions. Mo et al. [4] concluded that CFCSWs' performance is impacted by many variables, including axial load ratio, ratio of steel plate reinforcements, and shear connector spacing. They also indicated that an increased axial load will produce a more rapid loss of stiffness and strength than that of lower axial loads, while the presence of a higher steel plate ratio increases ductility and axial resistance. They also noted that if the spacing of shear connectors is too large, local buckling of the steel plates may occur in the elastic stage, negating the benefits of the composite system. These findings point to the need for careful detailing in connection design.

The ability to allow for innovative configurations has been researched by tampering with composite wall panels with L-shaped tooling for a composite wall edge region [5]. Results of cyclic testing have shown that composite walls were more effective than conventional reinforced concrete walls in dissipating energy and providing rigidity, among other structural properties. A second example of doing something a little different is the work of Xiao et al. [6], who studied embedded steel plate high-strength concrete (HSC) walls. Their 20-subject testing had conclusive evidence that the HSC walls improved the load, deformation, and energy dissipation capacities of normal RC walls. The optimum thresholds for design presented in the conclusion of the paper suggest that a control range for the steel ratio and maximum axial compression ratio of 0.5 should be maintained to ensure optimum seismic performance. Significant progress has been made toward developing accurate models for predicting the cyclic behavior of Composite Plate Shear Walls (C-PSW) and Concrete-Filled (CF) walls using numerical modeling techniques. Shafaei et al. [7] have produced results showing that it is both effective and efficient to develop simplified 2D FEM and fibre-based models using phenomenological effective stress-strain relationships to model C-PSW for the above-mentioned shapes. These simplified models will provide engineers with much-needed tools to easily and accurately simulate the earthquake response of C-PSW and CF walls.

Recent research has pushed the boundaries by incorporating advanced materials and investigating non-planar wall sections. Yang et al. [8] proposed a novel CSPSW where conventional concrete panels were replaced with Engineered Cementitious Composite (ECC) panels. Their nonlinear finite element analysis demonstrated that ECC panels, with their high tensile ductility and damage tolerance, provided superior restraint to the steel plate. The resulting system exhibited larger lateral stiffness and shear capacity than ordinary CSPSWs, with significantly reduced damage in both the steel plate and the cover panels.

For core-wall structures in high-rise buildings, C-shaped CSPSWs are critical. Kenarangi et al. [9] experimentally investigated the cyclic inelastic flexural behavior of large-scale C-shaped C-PSW/CF walls. Their findings were highly positive, demonstrating that the walls could develop their calculated plastic moment capacity and exhibited satisfactory cyclic performance under combined axial and lateral loads. This research provides vital validation for using C-PSW/CF as a primary lateral force-resisting system in complex, high-rise core-wall buildings.

A contemporary trend is the integration of high-strength materials to enhance economic efficiency and structural performance. Lou et al. [10] studied the seismic performance of shear walls using high-strength steel. Their pseudo-static tests revealed a nuanced trade-off: while increasing steel grade boosted bearing capacity and deformation capacity, it concurrently led to a reduction in ductility and energy dissipation capacity. This underscores the need for balanced design, potentially involving limits on steel ratio and axial compression ratio when utilizing high-strength steels to ensure adequate ductile performance under seismic demands.

The integration of Machine Learning (ML) and Artificial Neural Networks (ANN) offers a transformative paradigm shift for research on CSPSWs and other advanced structural systems. The validated high-fidelity finite element models (FEM) developed in the present study for CSPSW seismic analysis represent an excellent foundation for generating the extensive, high-quality datasets required to train such data-driven surrogate models. This approach directly addresses a critical challenge in computational structural engineering, where detailed nonlinear time-history or pushover analyses are accurate but prohibitively expensive for rapid design iteration or large-scale parametric studies. Machine learning models, including various ensemble and gradient boosting algorithms optimized with metaheuristic techniques, have demonstrated exceptional performance (with R^2 values often exceeding 0.95) in efficiently predicting complex structural responses such as the maximum inter-story drift ratio of steel diagrid systems, hysteretic curves of composite walls, and the flexural capacity of composite shear walls. Beyond mere prediction, advanced ML frameworks incorporate explainability tools like SHapley Additive exPlanations (SHAP), which provide vital insights into the relative importance and interactions of key design parameters, such as geometric dimensions, material strengths, and connector spacing, in determining structural behavior. This methodology creates a powerful synergy: the physical principles embedded in detailed FEMs ensure the data's fidelity, while the trained ML models offer engineers a rapid and reliable tool for performance assessment and design optimization. The pioneering work of researchers like Naeim et al. [11], Akbarzadeh et al. [12], and Jahangiri et al. [13] clearly demonstrates the pathway toward such integrated frameworks, which promise to significantly enhance the efficiency and scalability of performance-based seismic design for modern composite structural systems.

This research investigates the seismic behavior of steel-concrete composite shear walls under various earthquake records. A key focus is on optimizing the design by conducting a parametric study to determine the optimal spacing of shear connectors and the thickness of the concrete panel. The study aims to identify configurations that maximize energy dissipation and ductility while preventing premature local buckling of the steel plate, thereby establishing practical design guidelines for enhanced seismic performance.

2. Methodology

The numerical modeling section consists of four parts. Section 2.1 describes the constitutive models of the concrete and steel materials used in the numerical models. Section 2.2 presents the elements used, and Section 2.3 explains the contact interactions

between different parts and the applied loading. In Section 2.4, the validation of the numerical model against an experimental specimen is performed.

2.1. Material constitutive behavioral model

2.1.1. Concrete

The concrete damaged plasticity (CDP) model in ABAQUS was utilized to simulate the inelastic behavior of concrete under both compressive and tensile stresses. For the compressive response, the modified Hognestad model was employed to define the uniaxial stress-strain relationship. This model provides a robust representation of the concrete's nonlinear ascending branch and the post-peak strain-softening behavior. In the tensile regime, the stress-strain curve is linear up to the tensile strength. After cracking, the descending branch of the curve is modeled with a strain-softening response that gradually reduces the stress-carrying capacity to zero at the ultimate tensile strain. This study specifically uses a stress-crack width relationship to define the post-cracking behavior. By converting the crack width to an equivalent strain, a uniaxial stress-strain law for tension is derived and implemented in the model.

The plasticity parameters of the CDP model were carefully calibrated. The flow potential function, which governs the direction of plastic flow, was defined using the Drucker-Prager hyperbolic function. The dilation angle, which controls the volume change under plastic deformation, was set to 40°. Furthermore, other key parameters were specified as follows: the eccentricity of the plastic potential surface was 0.1, the ratio of the biaxial to uniaxial compressive strength (f_{b0}/f_{c0}) was 1.16, and the shape factor for the yield surface (K_c) was 0.667. These parameters collectively ensure an accurate representation of the concrete's pressure-dependent yielding and failure [14, 15].

To mitigate convergence difficulties associated with strain-softening material models, a viscosity parameter was incorporated. This parameter introduces a slight rate-dependence into the constitutive equations, which helps regularize the problem and improves the convergence rate of the implicit analysis. For this model, a viscosity coefficient of 0.01 was adopted. This value provides sufficient numerical stabilization without significantly compromising the quasi-static nature of the study, thereby ensuring a robust and efficient solution process for simulating the complex fracture and crushing of concrete [16-20].

2.1.2. Steel plate, rebar, and shear stud

To accurately simulate the hysteretic behavior of the steel reinforcement under cyclic loading, a combined isotropic-kinematic hardening model was implemented in ABAQUS. This model accounts for both the Bauschinger effect and the evolution of the yield surface size. The kinematic hardening component, which governs the translation of the yield surface, was defined using three backstress components in the Chaboche formulation with the following specific parameters: the first backstress (α_1) had an initial modulus C_1 = 20,000 MPa and a saturation rate γ_1 = 500; the second backstress (α_2) was defined with C_2 = 1,500 MPa and γ_2 = 50; and the third backstress (α_3) with C_3 = 100 MPa and γ_3 = 5. Concurrently, the isotropic hardening component, which controls the expansion of the yield surface, was specified such that the initial yield stress of 240 MPa saturated to a maximum of 370 MPa, modeled with an exponential law defined by a hardening modulus $Q\infty$ = 150 MPa and a saturation exponent b = 5. This combined formulation enabled the model to replicate key cyclic phenomena, including a reduced compressive yield stress of approximately 200 MPa following initial tensile yielding and the progressive shifting of hysteresis loops, which was crucial for the seismic assessment performed in this study.

2.2. Elements

The structural components of the shear wall system were discretized using element formulations appropriate to their geometric and mechanical characteristics. The steel components, namely the shear wall plate and the boundary elements, were modeled with S4R shell elements. This element type is a 4-node, reduced-integration finite membrane-strain shell element that is highly effective for simulating thin-walled steel sections. Its formulation accounts for both bending and membrane stresses and can capture large-rotation behavior and the potential for buckling, making it an optimal choice for modeling the complex response of steel plates under in-plane and out-of-plane loads [21-24].

The concrete panel was simulated using C3D8R solid elements, which are 8-node linear bricks with reduced integration. This element is the standard for modeling massive, three-dimensional continuum structures like concrete, as it can accurately represent the state of stress within the volume of the panel. The reinforcement, including both longitudinal and transverse rebars embedded within the concrete panel, as well as the shear connectors, was modeled using T3D2 elements. These are 2-node, 3-dimensional truss elements that resist only axial forces. An embedded constraint technique was employed, whereby the T3D2 truss elements are embedded within the mesh of C3D8R solid elements, ensuring a perfect bond that simulates the composite action between the concrete and the steel reinforcement, while efficiently neglecting the more complex local bond-slip effects for a global structural analysis [25-27]. Fig. 1 illustrates the geometric specifications, boundary conditions, and types of elements employed in the numerical model.

A mesh sensitivity analysis was conducted to ensure the numerical robustness of the results, particularly for phenomena such as local buckling, concrete cracking, and shear stud action, which are known to be mesh-dependent [28]. Three distinct global mesh sizes were investigated for the concrete panel and the steel plate: a coarse mesh of 100 mm, a medium mesh of 50 mm, and a fine mesh of 25 mm. The key seismic performance parameters, including the initial elastic stiffness, the peak load-bearing capacity, and the cumulative energy dissipation under cyclic loading, were compared across these mesh densities. The results, summarized in Table 1, indicate that the differences in response between the medium (50 mm) and fine (25 mm) meshes are negligible, with

variations of less than 2% in peak load and energy dissipation. The coarse mesh (100 mm) showed a more pronounced deviation, especially in predicting the post-peak softening behavior and localized damage patterns. Consequently, the medium mesh size of 50 mm was selected for all subsequent analyses. This size provides an optimal balance between computational efficiency and result accuracy, ensuring that the findings are independent of the discretization choice.

Table 1. Results of the mesh sensitivity analysis.

Mesh size (mm)	Initial stiffness (kN/mm)	Peak load (kN)	Energy dissipation (kJ)
Coarse (100)	84.1	562	42.5
Medium (50)	86.8	571	44.2
Fine (25)	87.1	573	44.3

Note: Values are from a monotonic pushover analysis of the validation specimen. The energy dissipation is calculated up to a top displacement of 40 mm.

2.3. Loading protocol and contact between the components

The numerical model incorporated several constraints and boundary conditions to accurately represent the structural system. The connections between the boundary elements were assumed to be rigid. A tie constraint was defined between the steel shear wall plate and the boundary element to ensure full compatibility and force transfer at their interface. The base of the two boundary elements was fully fixed against translational movement in all three global directions. To prevent out-of-plane buckling and enforce a state of plane stress, the top of the boundary element was restrained in the direction perpendicular to the web of the wall. Both monotonic and cyclic displacement-controlled loading protocols were applied to the top of the boundary element to investigate the system's hysteretic response.

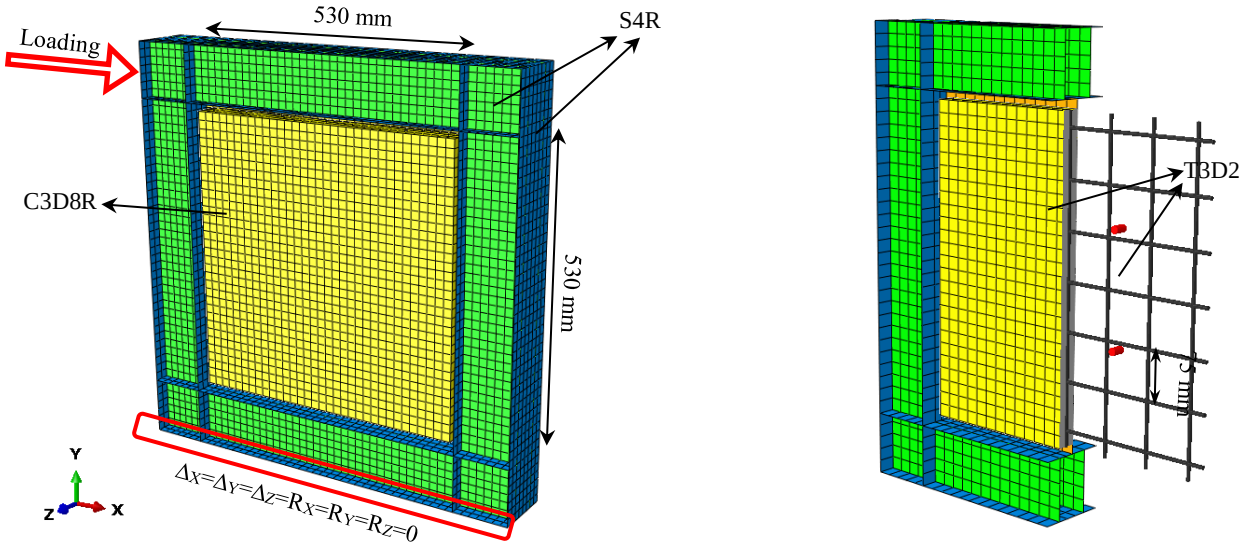

a) Dimensions and elements of the model b) Transverse cut to show the rebars and shear studs

Fig. 1. FE model detail.

2.4. Validation of the numerical model

In the present study, to validate the numerical model, the experimental investigation conducted by Arabzadeh et al. [29] was used in 2011. The CS specimen was considered among the experimental specimens. The beam and column elements were of type 2IPE100, and the steel plate infill had a thickness of 2 mm. The reinforcing bars inside the concrete panel had a diameter of 3 mm and were spaced 50 mm apart. The thickness of the concrete panel was 30 mm, and the concrete cover on the rebars was considered 15 mm. The yield stresses of the steel materials used in the column and beam were 361 MPa and 510 MPa, respectively. The yield stress and ultimate stress of the steel infill plate material were 268 MPa and 415 MPa, respectively.

Fig. 2 presents a comparison between the results of the laboratory specimen and the finite element model. The initial elastic stiffness of the experimental specimen was 85 kN/mm, while the value of this parameter in the numerical model was obtained as 87 kN/mm. Furthermore, the maximum load-bearing capacity in the experimental specimen was 585 kN, which was approximately 3% higher than that of the finite element model. In general, the behavior, failure mode, and seismic performance parameters of the experimental specimen and the numerical model show good agreement. Consequently, the employed material models, boundary conditions, and contact definitions between the various components of the system can be generalized for use in the numerical model.

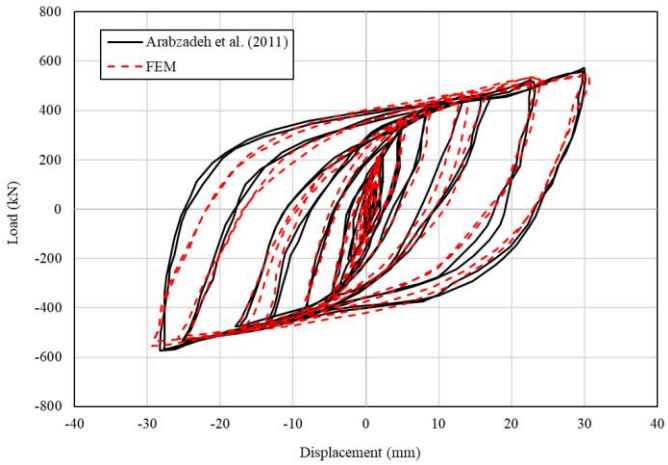

a) Load-displacement curves

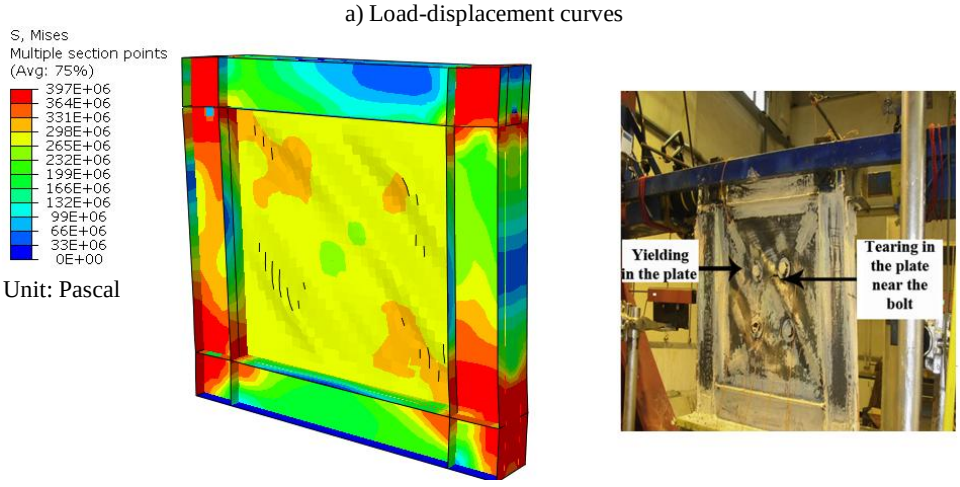

b) Failure mode of the test specimen [29] and the FE model

Fig. 2. Load-displacement curves and failure mode of the models.

3. Model definition

The design of the CSPSW followed a capacity-based methodology, as specific guidelines are codified in the Canadian standard [30]. The overarching principle was to concentrate inelastic deformation and energy dissipation in the steel infill plates, while ensuring the boundary beams and columns possess sufficient strength to remain essentially elastic under forces generated by the yielding infills. The concrete panel was detailed according to AISC 341-10 [31], with a specified thickness of 200 mm and a minimum reinforcement ratio of 0.0025, with bar spacing not exceeding 450 mm. The boundary members were specifically designed to withstand the full development of the tension field yield force in the steel plates. This tension field action, as described by Astaneh-Asl [32], becomes fully active after the concrete panel disintegrates under severe loading, a key behavioral aspect of C-PSWs where the concrete initially provides buckling restraint to the steel infill.

To investigate the behavior of the composite steel plate shear wall, two models-a four-story and a six-story structure-were utilized. The vertical boundary elements for the four-story and six-story frames were selected as IPB350 and IPB550 sections, respectively. The horizontal boundary elements in both frames were of type IPB250. A steel infill plate with a thickness of 5 mm was used. The concrete panel had a thickness of 200 mm and was reinforced with a grid of 6 mm diameter bars spaced at 300 mm. A 50 mm gap was provided between the concrete panel and the boundary elements. The compressive strength of the concrete panel was designated as 40 MPa.

To ensure a consistent and code-compliant seismic assessment, a set of seven ground motion records was selected (Table 2). These records were scaled independently for the four-story and six-story frames to account for their distinct dynamic characteristics. The scaling procedure adhered to the principles outlined in ASCE 7-16 [33]. For each frame, the individual records were scaled such that the average value of their 5% damped response spectra does not fall below 1.0 times the target spectrum, which was defined based on the site-specific seismic hazard, over a period range of 0.2T to 1.5T, where T represents the fundamental period of the respective frame (Fig. 3) [34]. This period-based scaling ensures that the input ground motions impose a consistent and appropriate level of seismic demand, tailored to the dynamic properties of each structure, thereby facilitating a meaningful comparison of their seismic performance. The scaling was performed to enable the calculation of the mean structural response from the suite of records, as this approach provides a more robust and reliable estimate of the expected seismic behavior than using a single record.

Table 2. Features of ground motions.

Earthquake	Abbreviation	Magnitude	Station	PGA (g)	PGV (cm/s)	Scaling factor (4-story)	Scaling factor (6-story)
Imperial Valley-06, 1979	IV	6.53	El Centro Array #3	0.27	47.99	0.77	0.79
Loma Prieta, 1989	LP	6.93	APEEL 2 - Redwood City	0.27	53.62	0.86	0.93
Kocaeli, Turkey, 1999	KT	7.51	Ambarli	0.25	36.52	1.32	1.54
Chi-Chi, Taiwan, 1999	CT	7.62	CHY047	0.18	26.63	1.50	1.76
Tottori, Japan, 2000	TJ	6.61	SMN002	0.18	21.95	0.91	1.16
Darfield, New Zealand, 2010	DN	7.0	Christchurch Resthaven	0.26	62.18	0.67	0.84
Christchurch, New Zealand, 2011	CN	6.2	Christchurch Resthaven	0.37	48.27	0.88	1.08

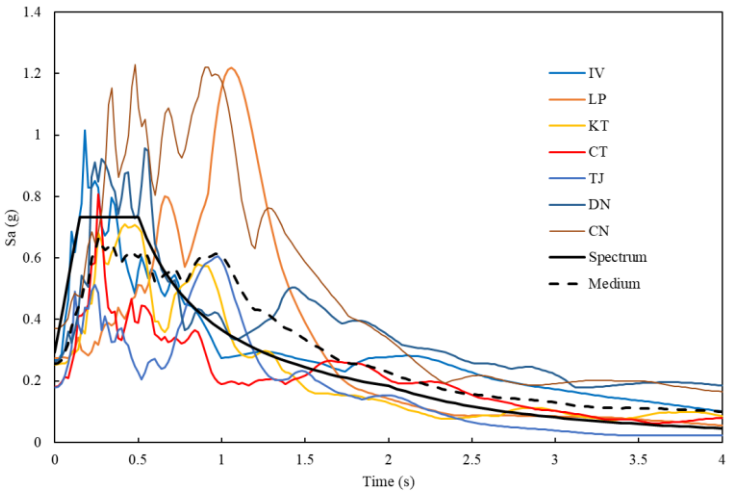

Fig. 3. Elastic spectra of seismic records.

4. Results and discussions

According to Fig. 4, non-linear time history analyses performed in ABAQUS for the 4-story CSPSW recorded maximum base reactions of 5152 kN, 4267 kN, 4912 kN, 4767 kN, 5237 kN, 4613 kN, and 4870 kN under the IV, LP, KT, CT, TJ, DN, and CN earthquakes, respectively. In comparison, the corresponding reactions for the 6-story CSPSW were 4762 kN, 4937 kN, 6054 kN, 5832 kN, 4812 kN, 5026 kN, and 5967 kN. The non-linear time history analyses revealed that the nominal shear strength of 3768 kN, calculated per AISC 341-10, significantly underestimated the actual dynamic response. For the 4-story and 6-story CSPSWs, the nominal strength was 28 and 37% lower than the peak dynamic base shears of 5237 kN and 6054 kN, respectively. This discrepancy is attributed to the load-sharing contributions of structural elements not considered in the code's simplified equation. The boundary steel columns provided a substantial portion of the system's shear resistance, with peak contributions of 25-26% and average contributions of 22 and 18% for the 4-story and 6-story frames, respectively. Furthermore, the reinforced concrete (RC) panels made a significant contribution to the overall strength, with their influence being most pronounced at the first story and diminishing progressively at higher levels. These findings demonstrate that the current design methodology, which ignores the capacity of boundary columns and RC panels, results in a conservative estimate of the system's true lateral strength.

According to Figs. 5 and 6, the analysis of axial forces and bending moments in the boundary column of the 4-and 6-story CSPSW under various earthquake records reveals a consistent internal force distribution pattern, albeit with significant variation in magnitude. Axial forces demonstrate a predictable accumulation from the top to the base, with the maximum compressive force reaching 15,993.6 kN under the IV ground motion, indicating the substantial global overturning moment demand on the column. Conversely, bending moments do not exhibit a monotonic increase and are often most severe at the column base, peaking at 1,114.83 kN-m under the DN earthquake. This peak moment at the base, coupled with the high concurrent axial force, defines the critical design scenario for the column. The significant scatter in both axial and moment values across different earthquakes, such as the notably lower forces under the CN record, underscores the critical influence of ground motion characteristics on the inelastic demand and highlights the necessity of a multi-record analysis to capture the full range of structural responses.

Preliminary parametric analyses indicate that increasing steel plate thickness or enlarging beam and column sections increases the share of lateral load resisted by the steel plate and boundary elements, whereas thickening the concrete panel primarily enhances local buckling restraint without significantly affecting global shear distribution. These trends clarify the sensitivity of component-level load sharing to geometric and material variations and provide practical insight for CSPSW design optimization.

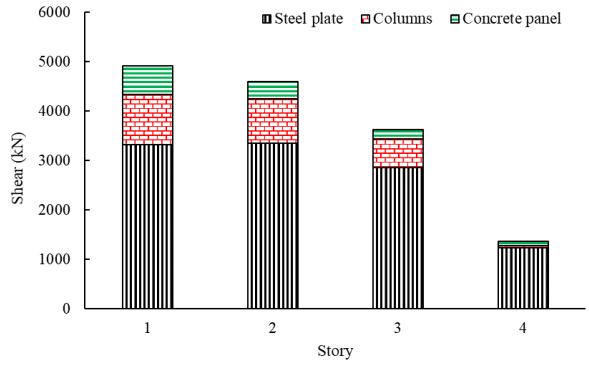

a) 4-story under KT record

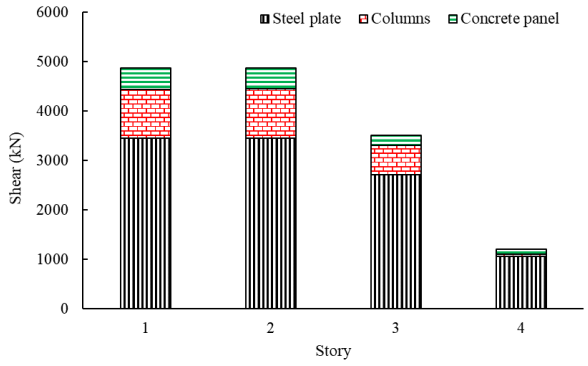

b) 4-story under CN record

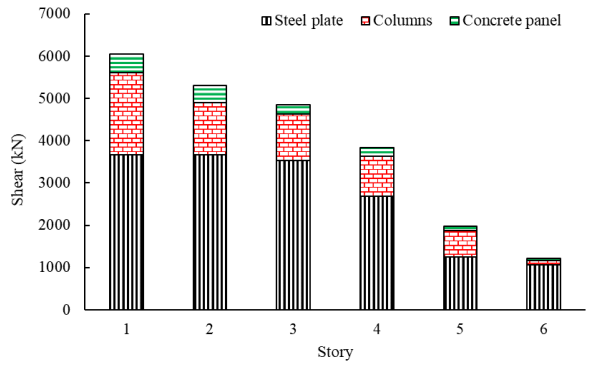

c) 6-story under KT record

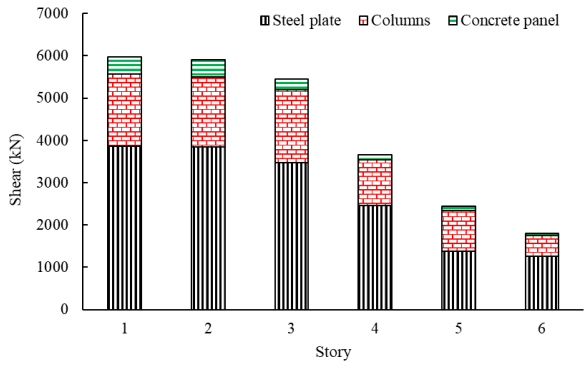

d) 6-story under CN record

Fig. 4. Peak story shear contribution for different components of 4- and 6-story.

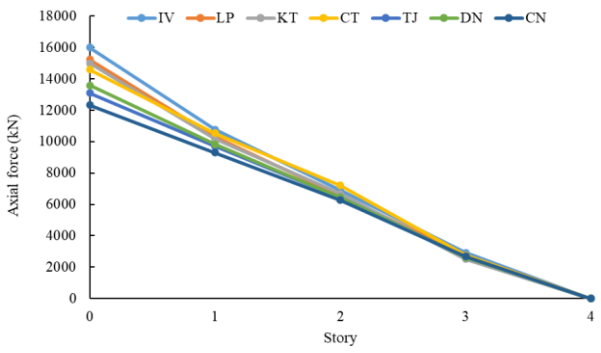

a) Axial force distribution

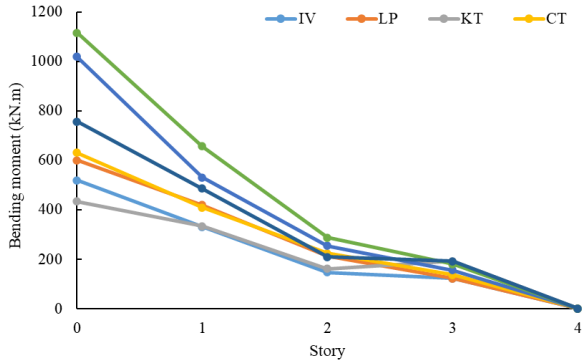

b) Bending moment distribution

Fig. 5. Axial force and bending moment at the column in the 4-story model.

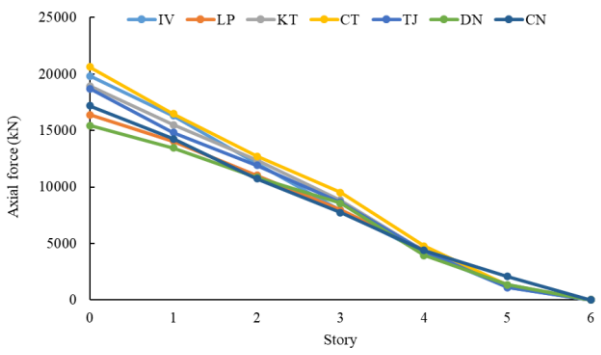

a) Axial force distribution

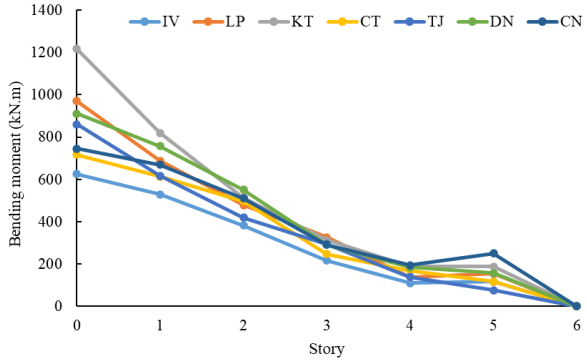

b) Bending moment distribution

Fig. 6. Axial force and bending moment at the column in the 6-story model.

Fig. 7 depicts the story displacement envelopes, recorded at the occurrence of maximum top-story displacement, illustrating the lateral deformation patterns induced by the selected suite of ground motions. The displacement profiles show a consistent increase along the height, confirming the expected flexural behavior. However, the significant scatter in values, particularly at the roof level (e.g., 68.4 mm vs. 119.6 mm for the 4-story frame), underscores the strong influence of ground motion frequency content on the structural response and the necessity for a multi-record design approach.

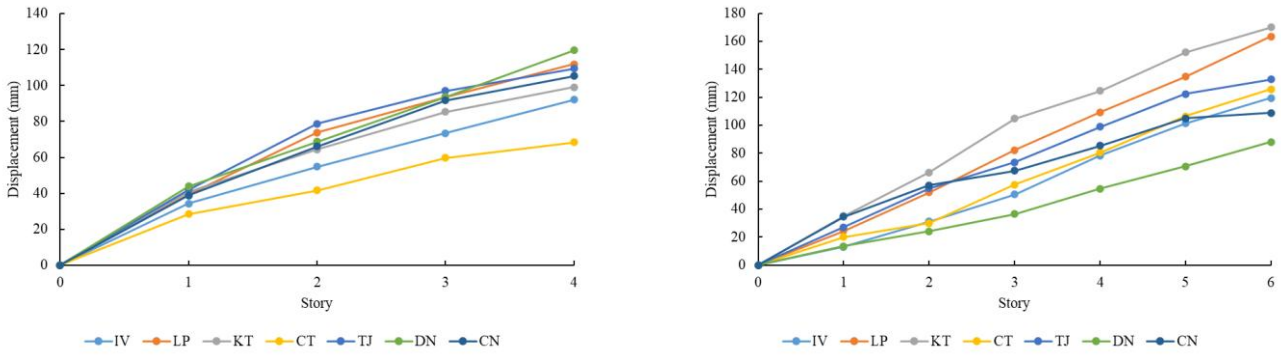

a) 4-story b) 6-story

Fig. 7. Distribution of displacement at the height of the models.

It should be noted that the observed underestimation of dynamic shear strength by AISC 341-10, quantified as 28–37% in this study, is strictly associated with the specific composite steel plate shear wall configurations examined herein, namely the 4-story and 6-story frames with fixed plate thickness, aspect ratio, and boundary member stiffness. The magnitude of conservativeness in simplified design provisions is known to be influenced by key parameters such as wall height, steel plate slenderness, and the relative stiffness of boundary elements. Therefore, the findings of this study should not be interpreted as a generalized limitation of the AISC provisions, but rather as evidence that, for the investigated configurations, the load-sharing contributions of boundary columns and reinforced concrete panels can be significant and are not explicitly accounted for in the current design formulation. Further parametric investigations are required to assess the extent of this behavior across a broader range of geometric and structural characteristics.

5. Determining the optimum shear stud spacing

To prevent local shear buckling of the steel plate before it yields, the elastic critical buckling stress must exceed the material's shear yield stress. For a composite plate shear wall, the concrete infill acts as a series of vertical and horizontal stiffeners at the shear stud lines, creating smaller subpanels. The refined elastic critical shear buckling stress for composite panel subpanels accounts for rotational stiffness at boundaries and concrete confinement effects:

$$\tau_{crl}^{*} = \eta_c \eta_s \frac{K_{sl}^{*} \pi^2 E}{12(1-\nu^2)} \left(\frac{t}{c}\right)^2 \tag{1}$$

Where $K_{sl}^{*} = 8.98 + \frac{5.61}{\alpha^2} + \Delta K_{sl}(\beta_r)$ is the enhanced buckling coefficient, $\eta_c = 1 + 0.25\sqrt{f_c'/E_s}$ is the concrete confinement factor, $\eta_s = 0.9 + 0.1log(\beta_r)$ is the rotational stiffness factor. β_r is the rotational stiffness parameter, which is $\frac{k_{\theta c} 12(1-\nu^2)}{Et^3}$.

The refined spacing requirement ensures optimal performance:

$$c \leq \frac{t}{\sigma_y} \sqrt{\frac{K_{sl}^{*} \pi^2 E \eta_s \eta_c}{12(1-\nu^2)\sqrt{3} \times 1.1}} \tag{2}$$

For typical construction steel (E = 200,000 MPa, ν = 0.3):

$$c \leq 1855 \eta_s \eta_c \gamma_{sh} \tag{3}$$

For the studied CSPSWs (t = 5 mm, σ_y = 350 MPa, f'_c = 30 MPa):

The design calculations yielded a base allowable stud spacing of 495 mm to prevent local buckling. After applying corrections for concrete confinement ($\eta_c = 1.08$, increasing spacing to 535 mm) and boundary stiffness ($\eta_s = 0.95$, refining it to 508 mm), the final permissible spacing was established at approximately 510 mm. The implemented 300 mm spacing, therefore, provides a substantial safety margin of 1.7, confirming a design that is both robust against buckling and maintains economic efficiency.

From a practical design perspective, the proposed buckling-based formulation can be directly used to establish rational shear stud spacing limits for composite steel plate shear walls. For typical mid-rise CSPSWs with steel plate thicknesses of 4–6 mm and normal-strength concrete panels, the analytical results indicate that stud spacing in the range of approximately 300–500 mm is sufficient to ensure that elastic local buckling of the steel plate occurs after yielding. The lower bound of this range, as adopted in the present study, provides a clear safety margin against premature buckling while remaining compatible with common construction

practices, welding accessibility, and cost considerations. Compared with existing code-based spacing limits, which are often conservative and do not explicitly account for concrete confinement and boundary rotational stiffness, the proposed formulation enables designers to quantitatively assess the influence of material properties and detailing on buckling resistance, thereby supporting more transparent and efficient CSPSW design.

6. Conclusion

This study comprehensively investigated the seismic performance of composite steel plate shear walls through detailed numerical analysis.

- The current AISC 341-10 design methodology is conservative, underestimating the actual dynamic shear strength by 28-37%. This discrepancy arises because the code ignores the significant load-sharing contributions of the boundary columns and the reinforced concrete panel.
- Boundary columns provide substantial shear resistance, with peak contributions of 25-26% of the total base shear, highlighting their crucial role in the system's lateral load-resisting mechanism.
- The seismic response is highly sensitive to ground motion characteristics. A multi-record analysis is essential to capture the full range of structural demands, including the critical combination of high axial force and bending moment at the column base.
- A refined and scientifically rigorous methodology was developed to determine the maximum shear stud spacing, preventing local buckling before steel yielding. The implemented 300 mm spacing provides a safety margin of 1.7, confirming a robust and economical design.
- The validated finite element model demonstrates that CSPSWs exhibit excellent seismic performance through effective composite action, offering a reliable and efficient structural system for seismic regions.

Statements & Declarations

Author contributions

Mehdi Ebadi-Jamkhaneh: Conceptualization, Methodology, Formal analysis, Resources, Writing - Original Draft.

Funding

The authors received no financial support for the research, authorship, and/or publication of this article.

Data availability

The data presented in this study will be available on interested request from the corresponding author.

Declarations

The authors declare no conflict of interest.

References

[1] Ebadi Jamkhaneh, M., Ahmadi, M. Numerical and parametrical investigations of the behavior of composite steel plate shear walls with opening. Sharif Journal of Civil Engineering, 2021; 37.2: 13-23. doi:10.24200/j30.2020.54966.2689.

[2] Katrangi, M., Khanmohammadi, M. Seismic behavior of composite encased steel plate shear wall using experimental and numerical methods. Journal of Building Engineering, 2025; 114: 114477. doi:10.1016/j.jobe.2025.114477.

[3] Zhao, Q., Astaneh-Asl, A. Cyclic Behavior of Traditional and Innovative Composite Shear Walls. Journal of Structural Engineering, 2004; 130: 271-284. doi:10.1061/(ASCE)0733-9445(2004)130:2(271).

[4] Mo, J., Uy, B., Li, D., Thai, H.-T., Tran, H. A review of the behaviour and design of steel–concrete composite shear walls. Structures, 2021; 31: 1230-1253. doi:10.1016/j.istruc.2021.02.041.

[5] Kisa, M. H., Yuksel, S. B., Caglar, N. Experimental study on hysteric behavior of composite shear walls with steel sheets. Journal of Building Engineering, 2021; 33: 101570. doi:10.1016/j.jobe.2020.101570.

[6] Xiao, C., Zhu, A., Li, J., Li, Y. Experimental study on seismic performance of embedded steel plate-HSC composite shear walls. Journal of Building Engineering, 2021; 34: 101909. doi:10.1016/j.jobe.2020.101909.

[7] Shafaei, S., Varma, A. H., Broberg, M., Klemencic, R. Modeling the cyclic behavior of composite plate shear walls/concrete filled (C-PSW/ CF). Journal of Constructional Steel Research, 2021; 184: 106810. doi:10.1016/j.jcsr.2021.106810.

[8] Yang, X., Xu, L., Pan, J. Mechanical behavior of full-scale composite steel plate shear wall restrained by ECC panels. Journal of Building Engineering, 2021; 44: 102864. doi:10.1016/j.jobe.2021.102864.

[9] Kenarangi, H., Kizilarslan, E., Bruneau, M. Cyclic behavior of c-shaped composite plate shear walls – Concrete filled. Engineering Structures, 2021; 226: 111306. doi:10.1016/j.engstruct.2020.111306.

[10] Lou, G.-B., Chen, P.-X., Zheng, J.-H. Seismic performance of high-strength steel plate-concrete composite shear walls. Journal of Building Engineering, 2024; 82: 108258. doi:10.1016/j.jobe.2023.108258.

[11] Naeim, B., Javadzade Khiavi, A., Khajavi, E., Taghavi Khanghah, A. R., Asgari, A., Taghipour, R., Bagheri, M. Machine Learning Approaches for Fatigue Life Prediction of Steel and Feature Importance Analyses. Infrastructures, 2025; 10: 295. doi:10.3390/infrastructures10110295.

[12] Akbarzadeh, M. R., Naeim, B., Asgari, A., Estekanchi, H. E. Framework for multi-hazard parameterized fragility based uncertainty quantification and sensitivity analysis of offshore wind turbines. Soil Dynamics and Earthquake Engineering, 2026; 201: 109963. doi:10.1016/j.soildyn.2025.109963.

[13] Jahangiri, V., Akbarzadeh, M. R., Shahamat, S. A., Asgari, A., Naeim, B., Ranjbar, F. Machine learning-based prediction of seismic response of steel diagrid systems. Structures, 2025; 80: 109791. doi:10.1016/j.istruc.2025.109791.

[14] Ghassemieh, M., Rezapour, M. Finite Element Modeling of SMA-Confined Concrete: Influence of Winding Pitch and Temperature on Strength and Energy Dissipation. Civil Engineering and Applied Solutions, 2026; 2: 33-45. doi:10.22080/ceas.2025.30055.1042.

[15] Rezapour, M., Ghassemieh, M. Numerical Investigation of Fe-SMA Strengthened Masonry Walls under Lateral Loading. Civil Engineering and Applied Solutions, 2025; 1: 1-15. doi:10.22080/ceas.2025.29594.1022.

[16] Ebadi Jamkhaneh, M., Kafi, M. A., Kheyroddin, A., Shokri Amiri, M. Progressive collapse resistance of a composite steel and concrete structural frame. Proceedings of the Institution of Civil Engineers - Structures and Buildings, 2018; 172: 197-213. doi:10.1680/jstbu.17.00149.

[17] Ebadi Jamkhaneh, M., Ahmadi, M., Sadeghian, P. Simplified relations for confinement factors of partially and highly confined areas of concrete in partially encased composite columns. Engineering Structures, 2020; 208: 110303. doi:10.1016/j.engstruct.2020.110303.

[18] Ebadi-Jamkhaneh, M., Homaioon-Ebrahimi, A., N. Kontoni, D.-P. Numerical finite element study of strengthening of damaged reinforced concrete members with carbon and glass FRP wraps. Computers and Concrete, 2021; 28: 137-147. doi:10.12989/cac.2021.28.2.137.

[19] Ebadi-Jamkhaneh, M., Kontoni, D.-P. N., Homaioon Ebrahimi, A. Assessment of Different Methods for Enhancing Progressive Collapse Resistance of Irregular Reinforced Concrete Buildings Using Pushdown Analysis. Arabian Journal for Science and Engineering, 2024; 49: 13861-13883. doi:10.1007/s13369-024-08847-4.

[20] Ebadi-Jamkhaneh, M. Determining minimum non-connected concrete panel thickness and concrete type impact on seismic behavior of CSPSW. Structural Engineering and Mechanics, 2024; 91: 607-626. doi:10.12989/sem.2024.91.6.607.

[21] Ebadi Jamkhaneh, M., Ebrahimi, A. H., Shokri Amiri, M. Experimental and Numerical Investigation of Steel Moment Resisting Frame with U-Shaped Metallic Yielding Damper. International Journal of Steel Structures, 2019; 19: 806-818. doi:10.1007/s13296-018-0166-z.

[22] Koloo, F. A., Badakhshan, A., Fallahnejad, H., Jamkhaneh, M. E., Ahmadi, M. Investigation of Proposed Concrete Filled Steel Tube Connections under Reversed Cyclic Loading. International Journal of Steel Structures, 2018; 18: 163-177. doi:10.1007/s13296-018-0313-6.

[23] Ebadi Jamkhaneh, M., Homaioon Ebrahimi, A., Shokri Amiri, M. Investigation of the Seismic Behavior of Brace Frames with New Corrugated All-Steel Buckling Restrained Brace. International Journal of Steel Structures, 2019; 19: 1225-1236. doi:10.1007/s13296-018-00202-2.

[24] Homaioon Ebrahimi, A., Ebadi Jamkhaneh, M., Shokri Amiri, M. 3D Finite-Element Analysis of Steel Moment Frames Including Long-Span Entrance by Strengthening Steel Cables and Diagonal Concentrically Braced Frames under Progressive Collapse. Practice Periodical on Structural Design and Construction, 2018; 23: 04018025. doi:10.1061/(ASCE)SC.1943-5576.0000388.

[25] Azarbara, M., Madandoust, R. Numerical Investigation of Trapezoidally Corrugated Steel Shear Walls with Openings: Effects of Stiffeners and Corrugation Orientation. Civil Engineering and Applied Solutions, 2026; 2: 60-70. doi:10.22080/ceas.2025.29967.1041.

[26] Rahimi, M., Bargi, K., Rezapour, M. Balancing Cost and Seismic Performance: Rectangular vs. T-shaped Shear Walls in Steel Frame Tall Buildings. Civil Engineering and Applied Solutions, 2026; 2: 12-21. doi:10.22080/ceas.2025.30091.1043.

[27] Rahimi, M., Bargi, K. Comparative Evaluation of Seismic Behavior of T-Shaped versus Rectangular Concrete Shear Walls in High-Rise Buildings. Civil Engineering and Applied Solutions, 2025; 1: 16-26. doi:10.22080/ceas.2025.29715.1029.

[28] Asgari, A., Ranjbar, F., Bagheri, M. Seismic resilience of pile groups to lateral spreading in liquefiable soils: 3D parallel finite element modeling. Structures, 2025; 74: 108578. doi:10.1016/j.istruc.2025.108578.

[29] Arabzadeh, A., Soltani, M., Ayazi, A. Experimental investigation of composite shear walls under shear loadings. Thin-Walled Structures, 2011; 49: 842-854. doi:10.1016/j.tws.2011.02.009.

[30] Canadian Standards Association (CSA). CAN/CSA-S16-09: Limit states design of steel structures. Longueuil (QC): CSA; 2009.

[31] American Institute of Steel Construction (AISC). AISC 341-10: Seismic Provisions for Structural Steel Buildings. Farmington Hills (MI): AISC; 2010.

[32] Astaneh-Asl, A. Seismic Behavior and Design of Composite Steel Plate Shear Walls. 1st ed. Berkeley (CL): Structural Steel Educational Council (SSEC); 2002.

[33] Engineers, A. S. o. C. Minimum Design Loads and Associated Criteria for Buildings and Other Structures. 1st ed. Farmington Hills (MI): American Society of Civil Engineers (ASCE); doi:10.1061/9780784414248.

[34] Jahangiri, V., Naeim, B., Akbarzadeh, M. R., Asgari, A. Optimal intensity measures for resilience-oriented probabilistic seismic demand models of elevated steel tanks. Structures, 2025; 82: 110576. doi:10.1016/j.istruc.2025.110576.